



<b>Publication Year</b>	2018
<b>Acceptance in OA@INAF</b>	2020-10-12T12:40:41Z
<b>Title</b>	The starburst galaxy NGC 253 revisited by H.E.S.S. and Fermi-LAT
<b>Authors</b>	H. E. S. S. Collaboration; Abdalla, H.; Aharonian, F.; Ait Benkhali, F.; Angüner, E. O.; et al.
<b>DOI</b>	10.1051/0004-6361/201833202
<b>Handle</b>	<a href="http://hdl.handle.net/20.500.12386/27716">http://hdl.handle.net/20.500.12386/27716</a>
<b>Journal</b>	ASTRONOMY & ASTROPHYSICS
<b>Number</b>	617

# The starburst galaxy NGC 253 revisited by H.E.S.S. and *Fermi*-LAT

H.E.S.S. Collaboration, H. Abdalla<sup>1</sup>, F. Aharonian<sup>3,4,5</sup>, F. Ait Benkhali<sup>3</sup>, E.O. Angüner<sup>19</sup>, M. Arakawa<sup>40</sup>, C. Arcaro<sup>1</sup>, C. Armand<sup>23</sup>, M. Arrieta<sup>14</sup>, M. Backes<sup>8,1</sup>, M. Barnard<sup>1</sup>, Y. Becherini<sup>10</sup>, J. Becker Tjus<sup>11</sup>, D. Berge<sup>35</sup>, S. Bernhard<sup>12</sup>, K. Bernlöhr<sup>3</sup>, R. Blackwell<sup>13</sup>, M. Böttcher<sup>1</sup>, C. Boisson<sup>14</sup>, J. Bolmont<sup>15</sup>, S. Bonnefoy<sup>35</sup>, P. Bordas<sup>3</sup>, J. Bregeon<sup>16</sup>, F. Brun<sup>25</sup>, P. Brun<sup>17</sup>, M. Bryan<sup>9</sup>, M. Büchele<sup>34</sup>, T. Bulik<sup>18</sup>, T. Bylund<sup>10</sup>, M. Capasso<sup>27</sup>, S. Caroff<sup>28</sup>, A. Carosi<sup>23</sup>, S. Casanova<sup>20,3</sup>, M. Cerruti<sup>15</sup>, N. Chakraborty<sup>3</sup>, S. Chandra<sup>1</sup>, R.C.G. Chaves<sup>16,21</sup>, A. Chen<sup>22</sup>, S. Colafrancesco<sup>22</sup>, B. Condon<sup>25</sup>, I.D. Davids<sup>8</sup>, C. Deil<sup>3</sup>, J. Devin<sup>16</sup>, P. deWilt<sup>13</sup>, L. Dirson<sup>2</sup>, A. Djannati-Atai<sup>29</sup>, A. Dmytriiev<sup>14</sup>, A. Donath<sup>3</sup>, L.O'C. Drury<sup>4</sup>, J. Dyks<sup>32</sup>, K. Egberts<sup>33</sup>, G. Emery<sup>15</sup>, J.-P. Ernenwein<sup>19</sup>, S. Eschbach<sup>34</sup>, S. Fegan<sup>28</sup>, A. Fiasson<sup>23</sup>, G. Fontaine<sup>28</sup>, S. Funk<sup>34</sup>, M. Füßling<sup>35</sup>, S. Gabici<sup>29</sup>, Y.A. Gallant<sup>16</sup>, T. Garrigoux<sup>1</sup>, F. Gaté<sup>23</sup>, G. Giavitto<sup>35</sup>, D. Glawion<sup>24</sup>, J.F. Glicenstein<sup>17</sup>, D. Gottschall<sup>27</sup>, M.-H. Grondin<sup>25</sup>, J. Hahn<sup>3</sup>, M. Haupt<sup>35</sup>, G. Heinzelmann<sup>2</sup>, G. Henri<sup>30</sup>, G. Hermann<sup>3</sup>, J.A. Hinton<sup>3</sup>, W. Hofmann<sup>3</sup>, C. Hoischen<sup>33</sup>\*, T. L. Holch<sup>7</sup>, M. Holler<sup>12</sup>, D. Horns<sup>2</sup>, D. Huber<sup>12</sup>, H. Iwasaki<sup>40</sup>, A. Jacholkowska<sup>15</sup>†, M. Jamroz<sup>36</sup>, D. Jankowsky<sup>34</sup>, F. Jankowsky<sup>24</sup>, L. Jouvin<sup>29</sup>, I. Jung-Richardt<sup>34</sup>, M.A. Kastendieck<sup>2</sup>, K. Katarzyński<sup>37</sup>, M. Katsuragawa<sup>41</sup>, U. Katz<sup>34</sup>, D. Kerszberg<sup>15</sup>, D. Khangulyan<sup>40</sup>, B. Khélifi<sup>29</sup>, J. King<sup>3</sup>, S. Klepser<sup>35</sup>, W. Kluźniak<sup>32</sup>, Nu. Komin<sup>22</sup>, K. Kosack<sup>17</sup>, S. Krakau<sup>11</sup>, M. Kraus<sup>34</sup>, P.P. Krüger<sup>1</sup>, G. Lamanna<sup>23</sup>, J. Lau<sup>13</sup>, J. Lefaucheur<sup>17</sup>, A. Lemièrre<sup>29</sup>, M. Lemoine-Goumard<sup>25</sup>, J.-P. Lenain<sup>15</sup>, E. Leser<sup>33</sup>, T. Lohse<sup>7</sup>, M. Lorentz<sup>17</sup>, R. López-Coto<sup>3</sup>, I. Lypova<sup>35</sup>, D. Malyshev<sup>27</sup>, V. Marandon<sup>3</sup>, A. Marcowith<sup>16</sup>, C. Mariaud<sup>28</sup>, G. Martí-Devesa<sup>12</sup>, R. Marx<sup>3</sup>, G. Maurin<sup>23</sup>, P.J. Meintjes<sup>38</sup>, A.M.W. Mitchell<sup>3</sup>, R. Moderski<sup>32</sup>, M. Mohamed<sup>24</sup>, L. Mohrmann<sup>34</sup>, E. Moulin<sup>17</sup>, T. Murach<sup>35</sup>, S. Nakashima<sup>41</sup>, M. de Naurois<sup>28</sup>, H. Ndiyavala<sup>1</sup>, F. Niederwanger<sup>12</sup>, J. Niemiec<sup>20</sup>, L. Oakes<sup>7</sup>, P. O'Brien<sup>31</sup>, H. Odaka<sup>41</sup>, S. Ohm<sup>35</sup>\*, M. Ostrowski<sup>36</sup>, I. Oya<sup>35</sup>, M. Padovani<sup>16</sup>, M. Panter<sup>3</sup>, R.D. Parsons<sup>3</sup>, C. Perennes<sup>15</sup>, P.-O. Petrucci<sup>30</sup>, B. Peyaud<sup>17</sup>, Q. Piel<sup>23</sup>, S. Pita<sup>29</sup>, V. Poireau<sup>23</sup>, A. Priyana Noel<sup>36</sup>, D.A. Prokhorov<sup>22</sup>, H. Prokoph<sup>35</sup>, G. Pühlhofer<sup>27</sup>, M. Punch<sup>29,10</sup>, A. Quirrenbach<sup>24</sup>, S. Raab<sup>34</sup>, R. Rauth<sup>12</sup>, A. Reimer<sup>12</sup>, O. Reimer<sup>12</sup>, M. Renaud<sup>16</sup>, F. Rieger<sup>3,39</sup>, L. Rinchuso<sup>17</sup>, C. Romoli<sup>3</sup>, G. Rowell<sup>13</sup>, B. Rudak<sup>32</sup>, E. Ruiz-Velasco<sup>3</sup>, V. Sahakian<sup>6,5</sup>, S. Saito<sup>40</sup>, D.A. Sanchez<sup>23</sup>, A. Santangelo<sup>27</sup>, M. Sasaki<sup>34</sup>, R. Schlickeiser<sup>11</sup>, F. Schüssler<sup>17</sup>, A. Schulz<sup>35</sup>, U. Schwanke<sup>7</sup>, S. Schwemmer<sup>24</sup>, M. Seglar-Arroyo<sup>17</sup>, M. Senniappan<sup>10</sup>, A.S. Seyffert<sup>1</sup>, N. Shafi<sup>22</sup>, I. Shilon<sup>34</sup>, K. Shiningayamwe<sup>8</sup>, R. Simoni<sup>9</sup>, A. Sinha<sup>29</sup>, H. Sol<sup>14</sup>, F. Spanier<sup>1</sup>, A. Specovius<sup>34</sup>, M. Spir-Jacob<sup>29</sup>, Ł. Stawarz<sup>36</sup>, R. Steenkamp<sup>8</sup>, C. Stegmann<sup>33,35</sup>, C. Steppa<sup>33</sup>, I. Sushch<sup>1</sup>, T. Takahashi<sup>41</sup>, J.-P. Tavernet<sup>15</sup>, T. Tavernier<sup>17</sup>, A.M. Taylor<sup>35</sup>\*, R. Terrier<sup>29</sup>, L. Tibaldo<sup>3</sup>, D. Tiziani<sup>34</sup>, M. Tluczykont<sup>2</sup>, C. Trichard<sup>28</sup>, M. Tsiro<sup>16</sup>, N. Tsuji<sup>40</sup>, R. Tuffs<sup>3</sup>, Y. Uchiyama<sup>40</sup>, D.J. van der Walt<sup>1</sup>, C. van Eldik<sup>34</sup>, C. van Rensburg<sup>1</sup>, B. van Soelen<sup>38</sup>, G. Vasileiadis<sup>16</sup>, J. Veh<sup>34</sup>, C. Venter<sup>1</sup>, A. Viana<sup>3,43</sup>, P. Vincent<sup>15</sup>, J. Vink<sup>9</sup>, F. Voisin<sup>13</sup>, H.J. Völk<sup>3</sup>\*, T. Vuillaume<sup>23</sup>, Z. Wadiasingh<sup>1</sup>, S.J. Wagner<sup>24</sup>, P. Wagner<sup>7</sup>, R.M. Wagner<sup>26</sup>, R. White<sup>3</sup>, A. Wierzcholska<sup>20</sup>, A. Wörnlein<sup>34</sup>, R. Yang<sup>3</sup>\*, D. Zaborov<sup>28</sup>, M. Zacharias<sup>1</sup>, R. Zanin<sup>3</sup>, A.A. Zdziarski<sup>32</sup>, A. Zech<sup>14</sup>, F. Zefi<sup>28</sup>, A. Ziegler<sup>34</sup>, J. Zorn<sup>3</sup>, and N. Żywucka<sup>36</sup>

(Affiliations can be found after the references)

## ABSTRACT

**Context.** NGC 253 is one of only two starburst galaxies found to emit  $\gamma$ -rays from hundreds of MeV to multi-TeV energies. Accurate measurements of the very-high-energy (VHE) ( $E > 100$  GeV) and high-energy (HE) ( $E > 60$  MeV) spectra are crucial to study the underlying particle accelerators, probe the dominant emission mechanism(s) and to study cosmic-ray interaction and transport.

**Aims.** The measurement of the VHE  $\gamma$ -ray emission of NGC 253 published in 2012 by H.E.S.S. was limited by large systematic uncertainties. Here, the most up to date measurement of the  $\gamma$ -ray spectrum of NGC 253 is investigated in both HE and VHE  $\gamma$ -rays. Assuming a hadronic origin of the  $\gamma$ -ray emission, the measurement uncertainties are propagated into the interpretation of the accelerated particle population.

**Methods.** The data of H.E.S.S. observations are reanalysed using an updated calibration and analysis chain. The improved *Fermi*-LAT analysis employs more than 8 years of data processed using pass 8. The cosmic-ray particle population is evaluated from the combined HE-VHE  $\gamma$ -ray spectrum using NAIMA in the optically thin case.

**Results.** The VHE  $\gamma$ -ray energy spectrum is best fit by a power-law distribution with a flux normalisation of  $(1.34 \pm 0.14^{\text{stat}} \pm 0.27^{\text{sys}}) \times 10^{-13} \text{ cm}^{-2} \text{ s}^{-1} \text{ TeV}^{-1}$  at 1 TeV – about 40% above, but compatible with the value obtained in Abramowski et al. (2012). The spectral index  $\Gamma = 2.39 \pm 0.14^{\text{stat}} \pm 0.25^{\text{sys}}$  is slightly softer than but consistent with the previous measurement within systematic errors. In the Fermi energy range an integral flux of  $F(E > 60 \text{ MeV}) = (1.56 \pm 0.28^{\text{stat}} \pm 0.15^{\text{sys}}) \times 10^{-8} \text{ cm}^{-2} \text{ s}^{-1}$  is obtained. At energies above  $\sim 3$  GeV the HE spectrum is consistent with a power-law ranging into the VHE part of the spectrum measured by H.E.S.S. with an overall spectral index  $\Gamma = 2.22 \pm 0.06^{\text{stat}}$ .

**Conclusions.** Two scenarios for the starburst nucleus are tested, in which the gas in the starburst nucleus acts as either a thin or a thick target for hadronic cosmic rays accelerated by the individual sources in the nucleus. In these two models, the level to which NGC 253 acts as a calorimeter is estimated to a range of  $f_{\text{cal}} = 0.1$  to 1 while accounting for the measurement uncertainties. The presented spectrum is likely to remain the most accurate measurements until the Cherenkov Telescope Array (CTA) has collected a substantial set of data towards NGC 253.

**Key words.** Galaxies: starburst, Gamma rays: galaxies, astroparticle physics

## 1. Introduction

Starburst galaxies are characterised by their high star-formation rate (SFR) and gas-consumption times of 1 Gyr or less. The starburst phase typically lasts for a few hundred million years (see e.g. Kennicutt & Evans 2012; Krumholz 2014, and references therein). Supernova (SN) remnants are believed to be the main sources of the Galactic cosmic rays (CRs). Starburst galaxies with their enhanced SFR and SN rate provide a testbed to probe this paradigm. Furthermore, CRs are star-formation regulators and drive complex chemical reactions by penetrating deep into dense molecular cloud cores (e.g. Indriolo & McCall 2013). There is also increasing evidence that CRs play an important role in galaxy formation and evolution (Booth et al. 2013; Salem & Bryan 2014; Salem et al. 2016; Pakmor et al. 2016) by driving galactic winds along expanding magnetic loops (e.g. Breitschwerdt et al. 1991, 1993) that result from their excitation of a Parker instability in the disk (Parker 1966). In this process the CRs heat the outflowing gas through the non-linear Landau damping of the scattering Alfvén waves that are excited by the outward streaming CRs (e.g. Zirakashvili et al. 1996). This CR heating might even prevent low-mass star formation in regions of very high CR densities such as starburst galaxies (e.g. Papadopoulos & Thi 2013).

Observations of starburst galaxies at  $\gamma$ -ray energies provide a useful probe to test the physics of CRs in these objects: i) They permit inference on the efficiency with which kinetic energy released in SN explosions is channelled via relativistic particles into  $\gamma$ -rays. ii)  $\gamma$ -rays can be used to infer properties of the interstellar medium in starburst galaxies or probe energy partition between CRs, magnetic fields and radiation fields. iii) Finally,  $\gamma$ -ray measurements can be used as an independent probe to test the paradigm of CR acceleration in SN remnant shocks.

The two archetypical starburst galaxies NGC 253 and M82 have been discovered to emit  $\gamma$ -rays with energies ranging from hundreds of MeV to several TeV (Acero et al. 2009; VERITAS Collaboration et al. 2009; Fermi-LAT Collaboration et al. 2010). Subsequently, detailed spectral studies of NGC 253 at TeV energies (Abramowski et al. 2012, HESS12 in the following) and the systematic search for GeV  $\gamma$ -ray emission from a sample of star-forming galaxies with *Fermi*-LAT, including NGC 253 and M82 (Ackermann et al. 2012), have been presented. Recently, NGC 253 has also been studied at hard X-rays with *NuSTAR*, soft X-rays with *Chandra* and at radio wavelengths with *VLBA* (Wik et al. 2014). Broadband spectral energy distribution (SED) modelling is performed with different approaches, ranging from semi-analytical one-zone models as described in e.g. Eichmann & Becker Tjus (2016), to three-dimensional (3D) steady state models (e.g. Persic et al. 2008; Rephaeli et al. 2010) and the treatment of time and space-dependent injectors (e.g. Torres et al. 2012). Starburst galaxies are also discussed as one of the possible source classes contributing to the astrophysical neutrino excess seen by the IceCube collaboration (Aartsen et al. 2014). NGC 253 remains one of the weakest detected TeV  $\gamma$ -ray sources. After three years of improvements to the calibration, reconstruction and analysis, a re-analysis of the  $\gamma$ -ray data, including a re-evaluation of systematic uncertainties, is presented in this work. In addition, 8 years of *Fermi*-LAT data are analysed and the updated  $\gamma$ -ray spectrum from 60 MeV to more than

10 TeV is studied. As a result of both improvements, the discussion presented in HESS12 is revisited.

## 2. H.E.S.S. data analysis

### 2.1. H.E.S.S. data

H.E.S.S. is an array of imaging atmospheric Cherenkov telescopes located in the Khomas Highland of Namibia and detects cosmic  $\gamma$ -rays with energies ranging from  $\sim 0.1$  to  $\sim 100$  TeV. The data used in this work are identical to the data presented and analysed in HESS12. The observations carried out in 2005 and from 2007 to 2009 sum to 158 h of acceptance-corrected live time. NGC 253 has not been the target of new observations from H.E.S.S. since then. Significantly improved statistics would only be possible at the cost of unreasonably large amounts of observation time. For a detailed description of the instrument and data set, the reader is referred to the original publication. The differences and improvements of the analysis methods compared to HESS12 are highlighted where applicable.

### 2.2. H.E.S.S. analysis

The results presented here and in HESS12 are based on a semi-analytical model of air showers for the event reconstruction and background suppression (de Naurois & Rolland 2009). This *model analysis* provides an improved angular resolution and a much better sensitivity compared to the classical Hillas parameter-based analysis. It is, however, susceptible to imperfections in the detailed modelling of the instrument response. Since the original publication, a small misalignment of the camera's position with respect to the telescope dish was found. This was not fully taken into account in the HESS12 analysis but has been accounted for in newer versions of the analysis software. The improvements in the pointing model have been verified using optical star positions and by application to known, strong  $\gamma$ -ray sources. The misaligned cameras resulted in a broadening of the point-spread function (PSF) and introduced a shift of the main discrimination variable in the *model analysis*. This shift led to misclassifications of  $\gamma$ -rays as background and resulted in an underestimation of the  $\gamma$ -ray flux of NGC 253. The same behaviour was uncovered and accounted for during the analysis of N 157B in the Large Magellanic Cloud (H.E.S.S. Collaboration 2015, supplement). The cross-check analysis presented in HESS12 is not significantly affected by the imperfect pointing model. The resulting systematic difference in reconstructed  $\gamma$ -ray flux between the *model analysis* and the cross-check analysis was taken into account in the flux systematic uncertainty in HESS12. As the precision of the  $\gamma$ -ray spectrum presented in HESS12 was limited by the systematic flux uncertainty, and since the modelling of the camera positions were improved since then, a reanalysis of the NGC 253 H.E.S.S. data and revised VHE  $\gamma$ -ray spectrum using the same data set as used in HESS12 is presented.

#### 2.2.1. VHE $\gamma$ -ray spectrum

The data reanalysis was performed using the same analysis framework as in HESS12, namely the *model analysis* (de Naurois & Rolland 2009). An updated position, extension limit, light curve and  $\gamma$ -ray spectrum are derived. The source is detected with a slightly lower significance of  $7.2\sigma$  compared to  $8.4\sigma$  in HESS12. The updated source position is  $\text{RA} = 0^{\text{h}}47^{\text{m}}32.54^{\text{s}} \pm 0^{\text{m}}11.2^{\text{s}}$ ,

Send offprint requests to: H.E.S.S. collaboration,  
e-mail: [contact.hess@hess-experiment.eu](mailto:contact.hess@hess-experiment.eu);

\* Corresponding authors

† Deceased

Dec =  $-25^{\circ}17'25.4'' \pm 0'10.3''$  (J2000), which changed only marginally towards an even better agreement with the optical center of NGC 253 at RA =  $0^{\text{h}}47^{\text{m}}33.1^{\text{s}}$ , Dec =  $-25^{\circ}17'18''$ . With the PSF being understood better, a possible extension of the  $\gamma$ -ray source is constrained to  $\leq 1.4'$  at the  $3\sigma$  level compared to the previous limit of  $\leq 2.4'$ . The new  $\gamma$ -ray spectrum, extracted at the best-fit position, is well described by a single power law, depicted in Fig. 1. The spectral points are given in Table 2. The flux normalisation  $F_0(1 \text{ TeV}) = (1.34 \pm 0.14^{\text{stat}} \pm 0.27^{\text{sys}}) \times 10^{-13} \text{ cm}^{-2} \text{ s}^{-1} \text{ TeV}^{-1}$  is  $\sim 40\%$  higher, and the best-fit spectrum is with a spectral index of  $\Gamma = 2.39 \pm 0.14^{\text{stat}} \pm 0.25^{\text{sys}}$  somewhat softer but consistent within errors compared to HESS12, where a spectral index of  $\Gamma^{2012} = 2.14 \pm 0.18^{\text{stat}} \pm 0.30^{\text{sys}}$  and a normalisation at 1 TeV of  $F_0^{2012} = (9.6 \pm 1.5^{\text{stat}} (+5.7, -2.9)^{\text{sys}}) \times 10^{-14} \text{ TeV}^{-1} \text{ cm}^{-2} \text{ s}^{-1}$  were reported. Both spectral parameters are consistent within the previously estimated systematic uncertainties. The relative statistical errors are slightly reduced due to the higher reconstructed  $\gamma$ -ray flux. We note that the systematic uncertainties are now comparable to the statistical uncertainties.

### 2.2.2. Estimation of systematic uncertainties

In HESS12, systematic uncertainties were estimated using a cross-check analysis, which accounted for systematic differences of the calibration, reconstruction and background subtraction. As this cross-check analysis proved to be unaffected by the imperfections in the modelling of the camera positions described above, the updated analysis presented here is compared to the original cross-check analysis. In HESS12, the difference in the flux normalisation between the two analysis chains was found to be 50 %, while the re-analysed flux normalisations agree within 2 %. The difference of best-fit spectral indices is on the 10 % level. As a 2 % difference is likely not representative for the real systematic uncertainty caused by different calibration chains, event reconstruction and background subtraction procedures, additional tests for systematic effects within the primary analysis framework have been performed.

A test for systematic shifts in the reconstructed  $\gamma$ -ray flux caused by the run selection has been performed by applying the original data quality criteria (e.g. Aharonian et al. 2006) used in HESS12 in comparison to a revised data quality selection. We found the data selection has an impact on the reconstructed flux at a level of 10 % and 3 % in flux normalisation and spectral index, respectively, for this faint source.

The applied  $\gamma$ -ray selection cuts might also introduce systematic effects. To estimate the impact of the chosen cuts, the data set was analysed using two different cut configurations: one designed for a low-energy threshold and optimised for spectral studies (*Standard*), the other optimised for weak sources (like NGC 253) and morphological studies, with a higher energy threshold (*Faint*). The differences between the analyses with the two cut configurations are 5 % in the spectral index and 13 % in the normalisation, and represent an estimate of the systematic uncertainty associated to the specific choice of the cut configuration.

The atmosphere is an integral part of an imaging atmospheric Cherenkov telescope and varies over time. The assumed atmospheric density profile influences the amount of light predicted to be seen by each camera. The light yield is uncertain by  $\sim 10\%$  (Aharonian et al. 2006). In order to estimate the effect of this uncertainty on the spectral parameters, the fit was repeated using response functions that were shifted by  $\pm 10\%$  in energy. The

resulting uncertainties are 10 % and  $\pm 0.09$  for the flux normalisation and the spectral index, respectively.

All uncertainties obtained for the flux normalisation and spectral index are summarised in Table 1. The error bars for the H.E.S.S. flux points shown in Figure 1 only represent the statistical uncertainties. In this figure, the red shaded area indicates the combined statistical and systematic uncertainties of the best-fit power-law model. The black contour depicts the error region as derived in HESS12.

**Table 1.** Estimated systematic uncertainties of the H.E.S.S. observations towards NGC 253.

Origin of uncertainty	spectral index	normalisation
reconstruction, calibration & analysis	$\pm 0.19$	2 %
run selection	$\pm 0.07$	10 %
selection cuts	$\pm 0.11$	13 %
atmospheric modelling	$\pm 0.09$	10 %
<b>Total systematic uncertainty</b>	<b><math>\pm 0.25</math></b>	<b>19 %</b>

## 3. Fermi-LAT data analysis

Since the publication of HESS12, the dataset accumulated by *Fermi*-LAT has increased by a factor of two. In addition, the release of the pass 8 data products (Atwood et al. 2013) allows for an additional gain in sensitivity and performance, especially at the lower end of the *Fermi*-LAT energy range of around 100 MeV. As this is the energy region where differences between hadronic and leptonic emission processes are best visible, a new analysis of more than 8 years' *Fermi*-LAT data was performed.

### 3.1. Fermi-LAT data

*Fermi*-LAT observations towards NGC 253 were selected in the time period of MET 239557417 - MET 507108410 (corresponding to 04 Aug 2008 - 26 Jan 2017), more than 8 years in total and double the data that was used in HESS12. The standard *Fermi* Science Tools<sup>1</sup> were employed to carry out the data analysis. A square region-of-interest (ROI) of  $15^{\circ} \times 15^{\circ}$  was defined around the optical center of NGC 253. In order to suppress albedo background events from the Earth's limb, events arriving during times in which the ROI was observed under unfavourable zenith angles were not included in the analysis. Specifically, times in which the spacecraft was tilted more than  $52^{\circ}$  and in which the ROI was only observable at zenith angles  $> 90^{\circ}$  were neglected. To avoid biases due to energy-dispersion effects at low energies, a pre-selection of  $\gamma$  rays was performed that restricts the energy range to a minimum of 30 MeV.

The HE  $\gamma$ -ray light curve of NGC 253 was monitored with the high cadence long-term monitoring tool *FlaapLUC* (Lenain 2017) which did not reveal significant variability.

### 3.2. New HE $\gamma$ -ray spectrum

The spectral analysis was performed based on the P8\_R2\_v6 version of the post-launch instrument response functions (IRFs). Both front and back converted photons were selected. A binned likelihood analysis using the *glike* tool in the energy range from

<sup>1</sup>v10r0p5, <http://fermi.gsfc.nasa.gov/ssc>



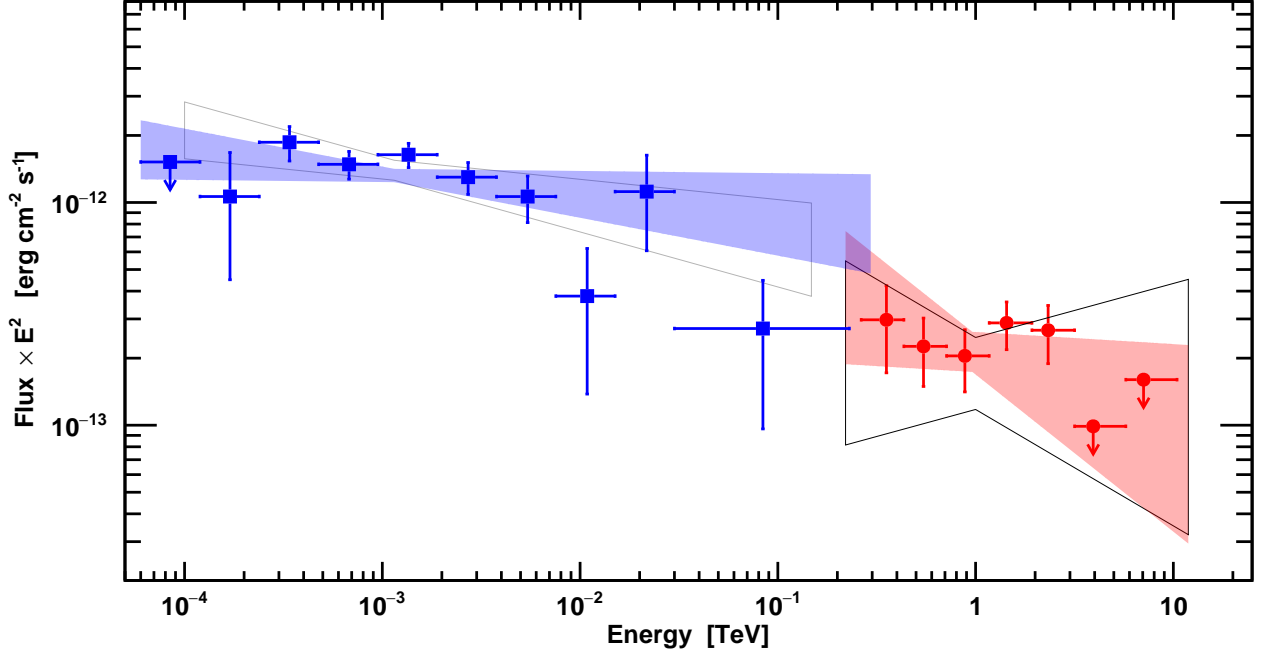


**Fig. 1.** H.E.S.S. and *Fermi*–LAT pass 8  $\gamma$ -ray SEDs are shown in red and blue, respectively. All error bars represent  $1\sigma$  statistical uncertainties. The upper limits are given at 95% confidence level. The red shaded area represents the  $1\sigma$  confidence region of the H.E.S.S. fit with combined statistical and systematic uncertainties. The black box shows the  $1\sigma$  confidence region of the H.E.S.S. fit from HESS12. The grey box shows the *Fermi*–LAT 3FGL best fit. We note that the *Fermi*–LAT measurement uncertainties are dominated by the low statistics. The systematic error of the *Fermi*–LAT points range from 5 % to 20 %. The blue area shows the best fit power-law to the *Fermi*–LAT pass 8 data.

60 MeV to 500 GeV was performed. All known sources as described in the 3FGL, as well as the diffuse galactic background *iso\_P8R2\_SOURCE\_V6* and the isotropic diffuse background  $\gamma$ -ray emission (*gll\_iem\_v06*) were included in the fit. The flux normalisations and spectral indices of all contributing sources in the ROI were left free during the fit. NGC 253 is detected with a TS value of 480, corresponding to roughly  $22\sigma$ . The flux above 60 MeV  $F(E > 60 \text{ MeV})$  is  $1.56 \pm 0.28^{\text{stat}} \pm 0.15^{\text{sys}} \times 10^{-8} \text{ cm}^{-2} \text{ s}^{-1}$ . Assuming the spectrum follows a power-law, the best-fit spectral index is  $2.09 \pm 0.07^{\text{stat}} \pm 0.05^{\text{sys}}$ .

To derive the SED, the energy range from 60 MeV to 30 GeV was divided into nine equally spaced  $\log_{10}(E)$  energy bins, while the higher-energy part from 30 GeV to 300 GeV was combined into a single bin due to the low count statistics at these energies. The fluxes obtained in these bins are shown in Fig. 1 and were obtained with a likelihood fit carried out in each bin accounting for the energy dispersion. The spectral points are given in Table 1. In the first energy bin ranging from 60 to 120 MeV NGC 253 is not detected significantly. Therefore an upper limit at a confidence level of 95% is derived. All higher-energy spectral points have TS values larger than 4, which corresponds to a significance of more than  $2\sigma$ . A photon with an energy of 214 GeV was detected within 0.1 degrees from NGC 253, which limits the highest-energy bin to 230 GeV. At energies above  $\sim 3 \text{ GeV}$ , the *Fermi*–LAT SED is very well described by a power-law extending into the entire H.E.S.S. energy domain. A power-law fit to all data points at energies above 3 GeV is found to yield a spectral slope of  $2.22 \pm 0.06^{\text{stat}}$ .

## 4. Results and Discussion of the combined HE- and VHE- gamma ray spectrum

### 4.1. Cosmic-ray luminosity and propagation in the starburst

From the combined *Fermi*–H.E.S.S.  $\gamma$ -ray observations in the energy range from 0.1 GeV to 3 TeV, the inferred integrated  $\gamma$ -ray luminosity is estimated to be  $L_\gamma = 1.19 \pm 0.35^{\text{stat}} \times 10^{40} \text{ erg s}^{-1}$ . Adopting a fiducial CR luminosity for the nucleus of the starburst galaxy region of  $L_{\text{CR}} = 10^{41} \text{ erg s}^{-1}$ , it is immediately apparent that of the order of  $\sim 10\%$  of such a CR luminosity must be transferred to  $\gamma$ -rays. The motivation for this fiducial CR luminosity comes from the inferred Milky Way’s CR luminosity, which is estimated to lie within the range  $0.6 - 3 \times 10^{41} \text{ erg s}^{-1}$  (Drury 2012).

Further consideration of the reference CR luminosity value for the starburst region comes from an estimation of the power fed into the CR population by SNe in this system,  $L_{\text{CR}} = \Theta E_{\text{SN}} \nu_{\text{SN}} \approx 1.6 \times 10^{41} \text{ erg s}^{-1}$ , where a fixed fraction  $\Theta \approx 0.1$  of the supernova remnant (SNR) kinetic power is fed into CRs, a total SNR kinetic energy  $E_{\text{SN}} = 10^{51} \text{ erg}$  is assumed to be released in each event, and the SNR rate within the starburst region of NGC 253 is  $\nu_{\text{SN}} \approx 0.05 \text{ yr}^{-1}$ , motivated from radio, infrared (IR), and optical observations of NGC 253 and taken from Engelbracht et al. (1998); Van Buren & Greenhouse (1994); Ohm & Hinton (2013) for the distance of 3.5 Mpc (Dalcanton et al. 2009, see HESS12). This estimated value is within the estimated range of  $(0.6 - 3) \times 10^{41} \text{ erg s}^{-1}$  for the CR luminosity of the Milky Way under the same assumptions (Drury 2012).

The rather hard overall differential  $\gamma$ -ray spectrum observed for this system up to the highest detected energies is an indication against diffusion-dominated transport of the CRs in the starburst region, a scenario which would be analogous to the conventional diffusion picture for diffuse CRs in the ISM of our Galaxy. Indeed, the high velocity of the starburst wind (see HESS12) rather suggests an advection-dominated transport, and therefore a spectrum of  $\gamma$ -rays emitted from the starburst region whose form is close to that of the source charged-particle spectrum, at least at energies above a few GeV, where the form of the hadronic  $\gamma$ -ray energy spectrum should roughly follow that of the generating charged particles. How closely the form of the  $\gamma$ -ray spectrum follows that of the CRs depends on the density of the gas in the starburst region. We consider two scenarios, which represent two extreme cases for this system.

If the gas in the system acts as a *thick* target, CRs will lose all their energy in the starburst region through  $pp$  interactions. In this regime, the rise of the  $pp$  interaction cross-section with energy softens the spectrum of CRs in the system relative to their source spectrum. This softening, however, is naturally compensated for by the  $\gamma$ -ray emission process itself, resulting in the photon index matching that of the source CR spectral slope. To ascertain the best-fit spectral slope for this case, a power-law fit to all data points from 3 GeV to 3 TeV was performed. This approach neglects the systematic uncertainties of both measurements, resulting in small statistical uncertainties on the obtained fit parameters. Energies below 3 GeV are not considered as the proton kinematics start to impact the results, leading to a departure from the power-law description at energies close to the pion production threshold. The best-fit spectral index was found to be  $2.22 \pm 0.06^{\text{stat}}$ .

If the gas in the starburst region is considered to be a *thin* target for CRs, particles are able to escape the starburst region via advection before losing a significant fraction of their energy. In this regime, the spectral slope of CRs in the system is not altered relative to that in their source. Once again, however, the growth of the  $pp$  cross-section with energy results in higher energy CRs more efficiently losing their energy than lower energy CRs, hardening the  $\gamma$ -ray spectrum produced. In turn, correcting for this over-representation of high energy  $\gamma$ -rays yields a CR spectrum that is softer than the  $\gamma$ -ray spectrum. In order to estimate the CR spectral shape under these assumptions, a description of starburst nucleus of NGC 253 as well as the inelastic proton scattering cross-section is necessary. The cross-section and branching ratios can be forward folded with a proton test distribution. A tool that allows for all of this is *NAIMA* (Zabalza 2015), a tool which employs the Markov Chain Monte Carlo methods from Goodman & Weare (2010) implemented in *emcee* (Foreman-Mackey et al. 2013). It fits the parameters of the proton test distributions based on the measured  $\gamma$ -ray spectrum, utilising the Kafexhiu et al. (2014) parameterisation of the  $pp$  interaction differential cross-sections. Assuming a distance of 3.5 Mpc (Dalcanton et al. 2009) and utilising the cross-section of the  $pp$  energy losses and pion production from PYTHIA 8, protons were simulated in a kinetic energy range from 0.1 GeV to 0.5 PeV according to a power-law in momentum with spectral index  $\alpha$  and normalisation  $N_0$  at the reference momentum  $p_0$  of the form

$$N(E) = \frac{N(p_0)}{\beta c} \times \left(\frac{p}{p_0}\right)^{-\alpha}, \quad (1)$$

where  $E$  is the total energy of the proton,  $p$  is the proton momentum, and  $\beta$  the proton velocity in units of  $c$ . The fit was done using both, the updated H.E.S.S. and *Fermi*–LAT spectrum, using statistical uncertainties only. Also, the upper limits are taken into account in the fit. The resulting best-fit spectral index obtained is  $\alpha = 2.46 \pm 0.03^{\text{stat}}$ . The  $\gamma$ -ray spectrum that is produced via pion decay from this proton distribution is depicted in Fig. 2. The  $\chi^2/N_{\text{dof}}$  of the best fit of 0.97 for 12 degrees of freedom, as well as the residuals indicate a good fit to the data. The total energy available in protons above a kinetic energy of 290 MeV (the pion production threshold) is  $(2.0 \pm 0.2^{\text{stat}}) \times 10^{53}$  erg.

Since the systematic uncertainties on the measured flux normalisation in the H.E.S.S. energy range are as large as the statistical ones, the fit was performed again by shifting the H.E.S.S. data points. For this, all measured flux points were increased (or decreased) by 20%. The resulting best fit parameters for the proton spectrum varied by  $\sim 3\%_{\text{H.E.S.S. norm}}^{\text{sys}}$  and  $\pm 0.03_{\text{H.E.S.S. norm}}^{\text{sys}}$  for the normalisation and the spectral index, respectively. Additionally, the impact of the exact choice of  $pp$ -interaction parameterisation was tested by repeating the fit using alternative descriptions of  $pp$ -interaction processes from QGSJET and SYBILL instead of PYTHIA8. We found that the choice of the parameterisation adds another uncertainty at the same level as the statistical ones, namely  $\sim 6\%_{\text{interaction}}^{\text{sys}}$  and  $\pm 0.03_{\text{interaction}}^{\text{sys}}$  for the flux normalisation and the spectral index respectively. If the H.E.S.S. measurement is excluded from the fit, the best-fit spectral index is around 2.6 and undershoots the H.E.S.S. measurement.

A limiting factor in the effort to recover the CR source spectrum comes from the complications introduced into the in-situ CR picture, from a consideration of the potential competing particle propagation and energy loss channels. The source spectrum will have an index between those obtained in the *thick* and *thin* one-dimensional (1D) models as long as convection dominates the particle propagation in the starburst region and only pion-decay  $\gamma$ -ray production matters.

#### 4.2. Cosmic-ray calorimetry in the starburst nucleus

The level at which the starburst system acts as a CR calorimeter,  $f_{\text{cal}}$ , is defined by the ratio of power that is channelled into pion production relative to the total amount of potential power available for pion production. A complete comparison of the calorimetric level therefore requires the further estimation of the fraction of CR energy in the population with energies above the threshold for pion production,  $f_{\pi}$ . We note that  $\gamma$ -ray observations are only sensitive to this high-energy component. As was discussed in HESS12,  $f_{\pi}$  is reasonably estimated with  $f_{\pi} \approx 3 - \Gamma$  (see Appendix in HESS12) which is based on the assumption of a simple power-law extrapolation of the CR momentum spectrum with index  $\Gamma$  over the whole particle energy range.

An estimation of the calorimetric level  $f_{\text{cal}} = L_{\pi}/L_{\text{CR}}(E_{\text{CR}} > E_{\pi}^{\text{th}})$  of the system, using the reference values and a value  $f_{\pi} \sim 0.66$ , intermediate between the two extreme cases  $\Gamma = 2.22$  and  $2.46$ , gives

$$f_{\text{cal}} \approx 0.34 \left(\frac{0.66}{f_{\pi}}\right) \left(\frac{L_{\gamma}}{1.2 \times 10^{40} \text{ erg s}^{-1}}\right) \left(\frac{1.6 \times 10^{41} \text{ erg s}^{-1}}{L_{\text{CR}}}\right), \quad (2)$$

where  $E_{\pi}^{\text{th}}$  is the threshold energy in  $pp$  collisions of CRs with the target gas, and the relation  $L_{\pi} = 3L_{\gamma}$  has been assumed.

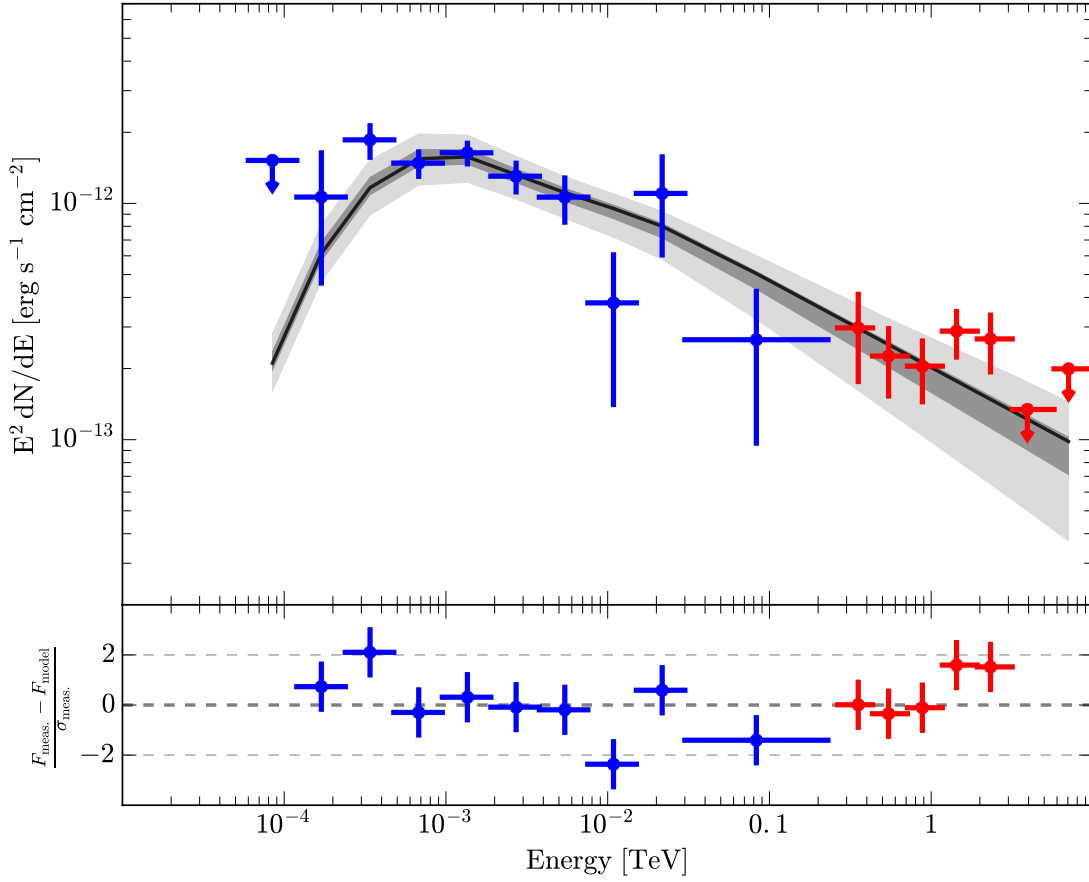


**Fig. 2.** The  $\gamma$ -ray SED obtained with H.E.S.S. and *Fermi*–LAT are shown together. In addition, the best-fit  $\gamma$ -ray spectrum from pion decay of inelastically scattered protons is shown as a black solid line. The grey shaded areas highlight the 1 and  $3\sigma$  confidence regions of the fit. The lower panel shows the residuals of the measurement with respect to the best fit, normalised to the measurements statistical uncertainty. Blue and red data points correspond again to the measurements obtained with *Fermi*–LAT and H.E.S.S., respectively.

It is important to note, however, that on top of the uncertainties in the determination of  $L_\gamma$ , considerable contributions to the uncertainty of this value exist in the determination of the luminosity of CRs with energies above the pion production threshold ( $f_\pi L_{\text{CR}}$ ).

The adoption of the extrema in the estimated range of the values  $L_\gamma$ ,  $L_{\text{CR}}$ , and  $f_\pi$  in Eq. 2 can be used to estimate the subsequent uncertainty range in the calorimetric value estimation,  $f_{\text{cal}}$ . These uncertainty contributions in its derivation collectively broaden the overall uncertainty, with the corresponding range of values obtained for NGC 253 being  $f_{\text{cal}} \approx 0.1 - 1$ . As part of this derivation, we impose a ceiling limit of 1, since values beyond this level are considered unphysical. This result highlights that only a crude order of magnitude estimation of the calorimetric value is presently possible. As such, this result is compatible with the estimate of Wang & Fields (2017) found using older HE and VHE  $\gamma$ -ray spectra in a more detailed calculation of the *thick* target scenario.

Furthermore, it should be noted that this level of uncertainty prevents a true estimation of the underlying uncertainty in  $L_{\text{CR}}$ , which is difficult to estimate in the absence of direct CR (and

their secondaries) observations in external galaxy systems. Our estimation of the level of uncertainty in this result should therefore be considered as a lower limit on this range, since these additional contributions would be expected to further broaden it. Such considerations highlight the difficulties faced in constraining the calorimetric value for starburst galaxies, and the essential role played by high-quality spectral measurements.

## 5. Conclusions

The observational and analysis results presented here strengthen the interpretation of the  $\gamma$ -ray emission in a hadronic scenario, as previously considered in Abramowski et al. (2012). Key supporting findings are based on the improved H.E.S.S. and *Fermi*–LAT analysis. The deeper understanding of the systematics at energies above 100 GeV help to better constrain the spectral shape. The *Fermi*–LAT pass 8 analysis and a factor two more statistics provide a more accurate measurement of the  $\gamma$ -ray emission in the energy range below 100 GeV.

The assumption that a population of protons is giving rise to the measured  $\gamma$ -ray spectrum through hadronic collisions pro-

vides an excellent fit to the data. Based on the presented analyses, the CR luminosity in the starburst nucleus was evaluated in two extreme scenarios assuming the gas to act as either a thin or thick target for the CRs. These two scenarios allowed us to bracket the CR luminosity in NGC 253 with uncertainties of one order of magnitude. The calorimetric level of NGC 253 was calculated to lie in the transition between the two scenarios with allowed values ranging from  $f_{\text{cal}} \approx 0.1$  to 1.

The presented spectra will remain the most precise measurements for the coming years. The VHE  $\gamma$ -ray spectrum will only be updated once the Cherenkov Telescope Array (CTA) has started operations and collected a sizeable set of observations towards NGC 253. The CTA measurement will provide more precise and detailed  $\gamma$ -ray data, potentially yielding an estimate of the extension of the region emitting VHE  $\gamma$ -rays. As demonstrated by [CTA Consortium \(2017\)](#) (their figure 11.4), the current gap in high-quality  $\gamma$ -ray data from 50 GeV to 200 GeV will be filled down to 100 GeV within 100 hours of observations. At higher energies, CTA will be able to probe the presence or absence of a cut-off of the  $\gamma$ -ray spectrum and therefore able to probe the acceleration limit of the astrophysical particle accelerators in the starburst nucleus or the onset of  $\gamma$ - $\gamma$  absorption in the dense radiation fields. Further significant improvements in the HE  $\gamma$ -ray domain will only be possible with missions like e-ASTROGAM, which could provide an accurate measurement in the energy range below 1 GeV ([De Angelis et al. 2017](#)) and probe the existence of a 'pion-bump' as predicted by hadronic emission models.

**Acknowledgements.** The support of the Namibian authorities and of the University of Namibia in facilitating the construction and operation of H.E.S.S. is gratefully acknowledged, as is the support by the German Ministry for Education and Research (BMBF), the Max Planck Society, the German Research Foundation (DFG), the Alexander von Humboldt Foundation, the Deutsche Forschungsgemeinschaft, the French Ministry for Research, the CNRS-IN2P3, the U.K. Science and Technology Facilities Council (STFC), the Knut and Alice Wallenberg Foundation the National Science Centre, Poland grant no. 2016/22/M/ST9/00382, the South African Department of Science and Technology and National Research Foundation, the University of Namibia, the National Commission on Research, Science & Technology of Namibia (NCRST), the Innsbruck University, the Austrian Science Fund (FWF), and the Austrian Federal Ministry for Science, Research and Economy, the University of Adelaide and the Australian Research Council, the Japan Society for the Promotion of Science and by the University of Amsterdam. We appreciate the excellent work of the technical support staff in Berlin, Heidelberg, Palaiseau, Paris, Saclay, and in Namibia in the construction and operation of the equipment. This work benefited from services provided by the H.E.S.S. Virtual Organisation, supported by the national resource providers of the EGI Federation.

## References

Aartsen, M. G., Ackermann, M., Adams, J., et al. 2014, *Physical Review Letters*, 113, 101101  
 Abramowski, A., Acero, F., Aharonian, F., et al. 2012, *The Astrophysical Journal*, 757, 158  
 Acero, F., Aharonian, F., Akhperjanian, A., et al. 2009, *Science*, 326, 1080  
 Ackermann, M., Ajello, M., Allafort, A., et al. 2012, *The Astrophysical Journal*, 755, 164  
 Aharonian, F., Akhperjanian, A. G., Bazer-Bachi, A. R., et al. 2006, *aap*, 457, 899  
 Atwood, W., Albert, A., Baldini, L., et al. 2013, *arXiv preprint arXiv:1303.3514*  
 Booth, C. M., Agertz, O., Kravtsov, A. V., & Gnedin, N. Y. 2013, *ApJ*, 777, L16  
 Breitschwerdt, D., McKenzie, J., & Völk, H. 1991, *Astronomy and Astrophysics*, 245, 79  
 Breitschwerdt, D., McKenzie, J., & Völk, H. 1993, *Astronomy and Astrophysics*, 269, 54  
 CTA Consortium. 2017, *Science with the Cherenkov Telescope Array*, arxiv:1709.07997  
 Dalcanton, J. J., Williams, B. F., Seth, et al. 2009, *ApJS*, 183, 67  
 De Angelis, A., Tatischeff, V., Tavani, M., et al. 2017, *Experimental Astronomy*, 44, 25

Min. - Mean - Max. Energy [TeV]	Energy Flux [erg s <sup>-1</sup> cm <sup>-2</sup> ]
(6.00 - 8.45 - 12.0) × 10 <sup>-5</sup>	< 1.52 × 10 <sup>-12</sup>
(1.20 - 1.70 - 2.39) × 10 <sup>-4</sup>	(1.06 ± 0.62) × 10 <sup>-12</sup>
(2.39 - 3.39 - 4.76) × 10 <sup>-4</sup>	(1.86 ± 0.33) × 10 <sup>-12</sup>
(4.76 - 6.79 - 9.50) × 10 <sup>-4</sup>	(1.48 ± 0.21) × 10 <sup>-12</sup>
(0.95 - 1.36 - 1.89) × 10 <sup>-3</sup>	(1.64 ± 0.20) × 10 <sup>-12</sup>
(1.89 - 2.72 - 3.78) × 10 <sup>-3</sup>	(1.30 ± 0.21) × 10 <sup>-12</sup>
(3.78 - 5.43 - 7.54) × 10 <sup>-3</sup>	(1.06 ± 0.25) × 10 <sup>-12</sup>
(0.75 - 1.09 - 1.50) × 10 <sup>-2</sup>	(3.79 ± 2.42) × 10 <sup>-13</sup>
(1.50 - 2.17 - 3.00) × 10 <sup>-2</sup>	(1.10 ± 0.51) × 10 <sup>-12</sup>
0.03 - 0.08 - 0.23	(2.65 ± 1.71) × 10 <sup>-13</sup>
0.26 - 0.35 - 0.43	(2.97 ± 1.25) × 10 <sup>-13</sup>
0.43 - 0.55 - 0.71	(2.26 ± 0.77) × 10 <sup>-13</sup>
0.71 - 0.88 - 1.17	(2.05 ± 0.64) × 10 <sup>-13</sup>
1.17 - 1.43 - 1.93	(2.88 ± 0.70) × 10 <sup>-13</sup>
1.93 - 2.33 - 3.17	(2.67 ± 0.78) × 10 <sup>-13</sup>
3.17 - 3.93 - 5.75	< 1.34 × 10 <sup>-13</sup>
5.75 - 7.07 - 10.4	< 1.99 × 10 <sup>-13</sup>

**Table 2.** The  $\gamma$ -ray spectral data as displayed in Figure 1 and 2. The *Fermi* and H.E.S.S. spectral points are separated by the horizontal line. The energy flux uncertainties correspond to the statistical uncertainties only. The flux limits are calculated for a confidence interval of 95 %.

de Naurois, M. & Rolland, L. 2009, *Astroparticle Physics*, 32, 231  
 Drury, L. O. 2012, *Astroparticle Physics*, 39, 52  
 Eichmann, B. & Becker Tjus, J. 2016, *ApJ*, 821, 87  
 Engelbracht, C., Rieke, M. J., Rieke, G. H., Kelly, D., & Achtermann, J. 1998, *The Astrophysical Journal*, 505, 639  
 Fermi-LAT Collaboration, Abdo, A. A., Ackermann, M., Ajello, M., & et al. 2010, *ApJ*, 709, L152  
 Foreman-Mackey, D., Hogg, D. W., Lang, D., & Goodman, J. 2013, *Publications of the Astronomical Society of the Pacific*, 125, 306  
 Goodman, J. & Weare, J. 2010, *Communications in applied mathematics and computational science*, 5, 65  
 H.E.S.S. Collaboration. 2015, *Science*, 347, 406  
 Indriolo, N. & McCall, B. J. 2013, *Chem. Soc. Rev.*, 42, 7763  
 Kafexhiu, E., Aharonian, F., Taylor, A. M., & Vila, G. S. 2014, *Phys. Rev.*, D90, 123014  
 Kennicutt, R. C. & Evans, N. J. 2012, *ARA&A*, 50, 531  
 Krumholz, M. R. 2014, *Physics Reports*, 539, 49  
 Lenain, J.-P. 2017, *Astrophysics Source Code Library*  
 Ohm, S. & Hinton, J. 2013, *Monthly Notices of the Royal Astronomical Society: Letters*, 429, L70  
 Pakmor, R., Pfrommer, C., Simpson, C. M., & Springel, V. 2016, *ApJ*, 824, L30  
 Papadopoulos, P. P. & Thi, W.-F. 2013, in *Advances in Solid State Physics*, Vol. 34, *Cosmic Rays in Star-Forming Environments*, ed. D. F. Torres & O. Reimer, 41  
 Parker, E. 1966, *The Astrophysical Journal*, 145, 811  
 Persic, M., Rephaeli, Y., & Arieli, Y. 2008, *A&A*, 486, 143  
 Rephaeli, Y., Arieli, Y., & Persic, M. 2010, *MNRAS*, 401, 473  
 Salem, M. & Bryan, G. L. 2014, *MNRAS*, 437, 3312  
 Salem, M., Bryan, G. L., & Corlies, L. 2016, *Monthly Notices of the Royal Astronomical Society*, 456, 582  
 Torres, D. F., Cillis, A., Lacki, B., & Rephaeli, Y. 2012, *MNRAS*, 423, 822  
 Van Buren, D. & Greenhouse, M. A. 1994, *The Astrophysical Journal*, 431, 640  
 VERITAS Collaboration, Acciari, V. A., Aliu, E., Arlen, T., & et al. 2009, *Nature*, 462, 770  
 Wang, X. & Fields, B. D. 2017, *Monthly Notices of the Royal Astronomical Society*, 474, 4073  
 Wik, D. R., Lehmer, B. D., Hornschemeier, A. E., et al. 2014, *ApJ*, 797, 79  
 Zabalza, V. 2015, *arXiv preprint arXiv:1509.03319*  
 Zirakashvili, V., Breitschwerdt, D., Ptuskin, V., & Völk, H. 1996, *Astronomy and Astrophysics*, 311, 113



- <sup>1</sup> Centre for Space Research, North-West University, Potchefstroom 2520, South Africa
- <sup>2</sup> Universität Hamburg, Institut für Experimentalphysik, Luruper Chaussee 149, D 22761 Hamburg, Germany
- <sup>3</sup> Max-Planck-Institut für Kernphysik, P.O. Box 103980, D 69029 Heidelberg, Germany
- <sup>4</sup> Dublin Institute for Advanced Studies, 31 Fitzwilliam Place, Dublin 2, Ireland
- <sup>5</sup> National Academy of Sciences of the Republic of Armenia, Marshall Baghramian Avenue, 24, 0019 Yerevan, Republic of Armenia
- <sup>6</sup> Yerevan Physics Institute, 2 Alikhanian Brothers St., 375036 Yerevan, Armenia
- <sup>7</sup> Institut für Physik, Humboldt-Universität zu Berlin, Newtonstr. 15, D 12489 Berlin, Germany
- <sup>8</sup> University of Namibia, Department of Physics, Private Bag 13301, Windhoek, Namibia
- <sup>9</sup> GRAPPA, Anton Pannekoek Institute for Astronomy, University of Amsterdam, Science Park 904, 1098 XH Amsterdam, The Netherlands
- <sup>10</sup> Department of Physics and Electrical Engineering, Linnaeus University, 351 95 Växjö, Sweden
- <sup>11</sup> Institut für Theoretische Physik, Lehrstuhl IV: Weltraum und Astrophysik, Ruhr-Universität Bochum, D 44780 Bochum, Germany
- <sup>12</sup> Institut für Astro- und Teilchenphysik, Leopold-Franzens-Universität Innsbruck, A-6020 Innsbruck, Austria
- <sup>13</sup> School of Physical Sciences, University of Adelaide, Adelaide 5005, Australia
- <sup>14</sup> LUTH, Observatoire de Paris, PSL Research University, CNRS, Université Paris Diderot, 5 Place Jules Janssen, 92190 Meudon, France
- <sup>15</sup> Sorbonne Université, Université Paris Diderot, Sorbonne Paris Cité, CNRS/IN2P3, Laboratoire de Physique Nucléaire et de Hautes Energies, LPNHE, 4 Place Jussieu, F-75252 Paris, France
- <sup>16</sup> Laboratoire Univers et Particules de Montpellier, Université Montpellier, CNRS/IN2P3, CC 72, Place Eugène Bataillon, F-34095 Montpellier Cedex 5, France
- <sup>17</sup> IRFU, CEA, Université Paris-Saclay, F-91191 Gif-sur-Yvette, France
- <sup>18</sup> Astronomical Observatory, The University of Warsaw, Al. Ujazdowskie 4, 00-478 Warsaw, Poland
- <sup>19</sup> Aix Marseille Université, CNRS/IN2P3, CPPM, Marseille, France
- <sup>20</sup> Instytut Fizyki Jądrowej PAN, ul. Radzikowskiego 152, 31-342 Kraków, Poland
- <sup>21</sup> Funded by EU FP7 Marie Curie, grant agreement No. PIEF-GA-2012-332350
- <sup>22</sup> School of Physics, University of the Witwatersrand, 1 Jan Smuts Avenue, Braamfontein, Johannesburg, 2050 South Africa
- <sup>23</sup> Laboratoire d'Annecy de Physique des Particules, Univ. Grenoble Alpes, Univ. Savoie Mont Blanc, CNRS, LAPP, 74000 Annecy, France
- <sup>24</sup> Landessternwarte, Universität Heidelberg, Königstuhl, D 69117 Heidelberg, Germany
- <sup>25</sup> Université Bordeaux, CNRS/IN2P3, Centre d'Études Nucléaires de Bordeaux Gradignan, 33175 Gradignan, France
- <sup>26</sup> Oskar Klein Centre, Department of Physics, Stockholm University, Albanova University Center, SE-10691 Stockholm, Sweden
- <sup>27</sup> Institut für Astronomie und Astrophysik, Universität Tübingen, Sand 1, D 72076 Tübingen, Germany
- <sup>28</sup> Laboratoire Leprince-Ringuet, Ecole Polytechnique, CNRS/IN2P3, F-91128 Palaiseau, France
- <sup>29</sup> APC, AstroParticule et Cosmologie, Université Paris Diderot, CNRS/IN2P3, CEA/Irfu, Observatoire de Paris, Sorbonne Paris Cité, 10, rue Alice Domon et Léonie Duquet, 75205 Paris Cedex 13, France
- <sup>30</sup> Univ. Grenoble Alpes, CNRS, IPAG, F-38000 Grenoble, France
- <sup>31</sup> Department of Physics and Astronomy, The University of Leicester, University Road, Leicester, LE1 7RH, United Kingdom
- <sup>32</sup> Nicolaus Copernicus Astronomical Center, Polish Academy of Sciences, ul. Bartycka 18, 00-716 Warsaw, Poland
- <sup>33</sup> Institut für Physik und Astronomie, Universität Potsdam, Karl-Liebknecht-Strasse 24/25, D 14476 Potsdam, Germany
- <sup>34</sup> Friedrich-Alexander-Universität Erlangen-Nürnberg, Erlangen Centre for Astroparticle Physics, Erwin-Rommel-Str. 1, D 91058 Erlangen, Germany
- <sup>35</sup> DESY, D-15738 Zeuthen, Germany
- <sup>36</sup> Obserwatorium Astronomiczne, Uniwersytet Jagielloński, ul. Orła 171, 30-244 Kraków, Poland
- <sup>37</sup> Centre for Astronomy, Faculty of Physics, Astronomy and Informatics, Nicolaus Copernicus University, Grudziadzka 5, 87-100 Torun, Poland
- <sup>38</sup> Department of Physics, University of the Free State, PO Box 339, Bloemfontein 9300, South Africa
- <sup>39</sup> Heisenberg Fellow (DFG), ITA Universität Heidelberg, Germany
- <sup>40</sup> Department of Physics, Rikkyo University, 3-34-1 Nishi-Ikebukuro, Toshima-ku, Tokyo 171-8501, Japan
- <sup>41</sup> Japan Aerospace Exploration Agency (JAXA), Institute of Space and Astronautical Science (ISAS), 3-1-1 Yoshinodai, Chuo-ku, Sagami-hara, Kanagawa 229-8510, Japan
- <sup>42</sup> Now at The School of Physics, The University of New South Wales, Sydney, 2052, Australia
- <sup>43</sup> Now at Instituto de Física de São Carlos, Universidade de São Paulo, Av. Trabalhador São-carlense, 400 - CEP 13566-590, São Carlos, SP, Brazil